NASA Technical Memorandum 83585

Ceramic Wear in Indentation and Sliding Contact

Kazuhisa Miyoshi and Donald H. Buckley
Lewis Research Center
Cleveland, Ohio

Prepared for the
Thirty-ninth Annual Meeting of the American Society of Lubrication Engineers
Chicago, Illinois, May 7–10, 1984

NASA

CERAMIC WEAR IN INDENTATION AND SLIDING CONTACT

Kazuhisa Miyoshi and Donald H. Buckley

National Aeronautics and Space Administration
Lewis Research Center
Cleveland, Ohio 44135

E-1884

ABSTRACT

This paper discusses the various wear mechanisms involved with single-crystal ceramic materials in indentation and in sliding contacts. Experiments simulating interfacial events have been conducted with hemispherical, conical and pyramidal indenters (riders).

With spherical riders, under either abrasive or adhesive conditions, two types of fracture pits have been observed. First, spherical-shaped fracture pits and wear particles are found as a result of either indenting or sliding. These are shown to be due to a spherical-shaped fracture along the circular or spherical stress trajectories. Second, polyhedral fracture pits and debris, produced by anisotropic fracture, are also found both during indenting and sliding. These are primarily controlled by surface and subsurface cracking along cleavage planes.

Several quantitative results have also been obtained from this work. For example, using a pyramidal diamond, crack length of Mn-Zn ferrite in the indentation process grows linearly with increasing normal load. Moreover, the critical load to fracture both in indentation and sliding is found to be directly proportional to the indenter radius.

Finally, the tangential forces present during sliding are very potent in producing conditions for fracture at the surface. Under such conditions, the observed anisotropy of friction and plastic deformation is explained on the basis of the primary slip systems of these ceramics.

INTRODUCTION

Since fracture is one of the main limitations to a wider use of ceramic materials in tribological applications, understanding and new developments in this area are particularly important. For example, conventional magnetic recording is accomplished by the relative motion of magnetic tape against a stationary (audio or computer) or rotating (video) read/write magnetic head. These heads are generally made of oxide ceramics such as Ni-Zn ferrite or Mn-Zn ferrite. For high-density, high-resolution recording, close proximity between the tape and the head is essential. The use of the ferrites in these applications strongly involve surface interactions. Cracking at and below the surface of ceramic oxides changes not only the characteristics of the head, but it also drastically affects the head life.

To reduce fracture wear in practical tribological applications, it is important to understand the various fracture wear mechanisms. If the mechanism of wear in a particular system can be identified, then some significant reduction in wear is often feasible.

This paper is principally concerned with a fundamental understanding of fracture wear of single-crystalline ceramics in indentation and sliding contact, and with demonstrating the most important intrinsic mechanisms determining fracture. The ceramic materials examined include SiC, MgO and Mn-Zn ferrite.

MICROFRACTURE IN INDENTATION CONTACT

When two solid surfaces are placed in contact, high pressures are developed in the regions where real contact occurs at the interface. If a hard particle or a hard asperity of approximately spherical shape is in contact with a ceramic under load, the ceramic initially deforms locally according to the well-known Hertzian elastic equation (ref. 1). Fractures with ring cracks have

been produced in flat-surfaced ceramics critically loaded, either statically or dynamically with hard spheres (refs. 2 to 7). In the present study, hemispherical diamond indenters with radii characteristic of asperities or wear particles were used to simulate real contact conditions.

Indenting with a hemispherical diamond indenter on a silicon carbide {0001} surface also results in the formation of circular (ring) cracks as well as in plastic deformation. Figure 1 presents scanning electron photomicrographs of the permanent indentations and the surrounding circular cracks generated by 0.1-, 0.02- and 0.008-mm-radius hemispherical diamond indenters. It becomes obvious from an examination of figure 1 that the plastic deformation is accompanied by nearly perfect circular cracking in the silicon carbide.

It is very interesting that, as shown in figure 1, the crystallinity of the solid does not influence the geometry of the cracks. In other words, for anisotropic solids such as a single crystal, some orientation dependence of the circular cracks produced in crystals with strong cleavage tendencies might be expected. Figure 1, however, reveals nearly circular cracks that were not crystallographically oriented.

Figures 1(b) and (c) also reveal cracks propagating and expanding radially from the center of the contact circle. The cracks form preferentially on the planes of easy cleavage in the silicon carbide. These photomicrographs clearly show several slip lines, accompanying plastic deformation, in the indentations. The slip lines are crystallographically oriented and are in the $\langle 11\bar{2}0 \rangle$ directions. To summarize, the indenting experiments generally revealed (1) a plastically deformed indentation, (2) circular cracks produced around the indentation without cleavage tendencies of a given crystal, and (3) radial cracks with strong cleavage tendencies for the given crystals.

Figure 2(a) is a scanning electron photomicrograph of an indentation on the single-crystal silicon carbide surface accompanied by an exceptionally

large fracture pit. The deformation and fracture made by the hemispherical indenter are also shown schematically in figure 2(b). Yet there are not confirmed criterions or reasonable data to explain what conditions can produce this exceptionally large fracture pit. The pit is, however, found in the indenting experiment which was conducted with a 0.008-mm-radius hemispherical diamond indenter at a load of 10N. There was a discharge of fragments that were displaced from the surface of the silicon carbide. The fracture pit is like a volcanic crater. The crater forms a wide basin with steeply sloping sides. The fracture pit (crater) contains a plastically deformed indentation in the center of the crater with small fracture pits. The crater is much larger than the indentation. The partially spherical surface in the crater and on the sides of the basin are all produced by the indenting and unloading actions of the diamond hemispherical indenter. There are many fracture steps on the surfaces of the spherical hillsides and on the sides of the basin. These steps may be due to sequential rupture of cohesive bonds along easy fracture planes such as the cleavage and quasi-cleavage planes. There are also many radial cracks on the nearly spherical fracture surface. The radial cracks are similar to those shown in figures 1(b) and (c).

Figure 3 presents scanning electron photomicrographs of indentations on a single-crystal magnesium oxide {001} surface (99.99 percent pure). The indenting experiments were conducted with the magnesium oxide in contact with a 0.02-mm-radius diamond indenter in air and in mineral oil with sulfur additive at a load of 0.25 N. The observed patterns of nearly circular cracks and crystallographically oriented cracks are much like those previously mentioned for silicon carbide.

The most prominent features of all of the crack patterns presented in figures 1 to 3 may be plausibly explained by reference to figure 4. When two solid surfaces are in contact, the stress concentration at the contact area may

produce a small zone of plastic deformation in the solid, as shown in figure 4. Cracks will subsequently be initiated in the solid. The cracks develop stable growth in a subsurface region and on the surface around the plastic deformation zone during the loading and unloading processes. The cracks, which are generally circular, spherical, and radial, are schematically shown in figure 4 with a model. As suggested by this schematic diagram, spherical cracks appear to develop along the spherical stress trajectories (refs. 7 to 9). Although crystallinity, however, is imposed on the crack geometries of anisotropic materials such as silicon carbide, it is possible that the cracks may grow and pile up in atomistic terms by the sequential rupture of cohesive bonds along the circular or spherical stress trajectories shown in figure 4.

MICROFRACTURE IN SLIDING CONTACT UNDER ABRASIVE CONDITIONS

If a tangential force is applied to the normally loaded hemisphere, the additional tangential stress compresses the ceramic and opposes the tensile tangential stress due to the normal load on the leading side of the rider. Conversely on the trailing side the tensile tangential stress is augmented. As a result, cracking will be restricted to the rear of the contact region and suppressed at the leading edge. Cracks of this type have long been observed when a hard hemisphere slides over the surface of a brittle solid (refs. 10 to 13).

In the present work, sliding friction experiments were conducted with a hemispherical diamond (0.02 mm radius) in contact with a flat either of silicon carbide or of Mn-Zn ferrite. Figure 5 presents scanning electron photomicrographs of wear tracks on these surfaces. As shown in these photomicrographs plastic deformation occurs in both the silicon carbide and the Mn-Zn ferrite. Two kinds of crack are observed. One occurs in the wear tracks and propagates perpendicular to the sliding direction. The other is primarily observed on

both sides of the wear track, propagating outward from the wear track. Two effects of potential importance for sliding contact will be considered:

(1) The deformation and fracture behavior of ceramic materials may be very dependent on crystallographic orientation;

(2) The cracks may grow easily by application of shearing force during sliding.

Effects of Crystallographic Orientation

Coefficient of friction and widths of the permanent grooves in plastic flow accompanied with surface cracking were measured as a function of the crystallographic direction of sliding on the {0001}, {10$\bar{1}$0}, and {11$\bar{2}$0} planes of SiC for the conical diamond rider in mineral oil. The apical angle of the conical rider was 117±1° and the radius of curvature at the apex was less than 5 μm. Mineral oil was used to minimize adhesion. Figure 6 indicates that the effects of crystallographic orientation on the coefficient of friction and groove width are correlated. Thus, the <11$\bar{2}$0> direction on the basal {0001} plane has the larger groove, primarily as a result of plastic flow and is the direction of high friction for this plane. The <0001> directions on the {10$\bar{1}$0} and {11$\bar{2}$0} planes have the greater groove width and likewise are the directions of high friction when compared with the <11$\bar{2}$0> on the {10$\bar{1}$0} plane and the <10$\bar{1}$0> on the {11$\bar{2}$0} plane (ref. 14).

The contact pressure calculated from the data of the groove width is also represented in figure 6, together with the Knoop hardness obtained by Shaffer (ref. 15). The anisotropies of this contact pressure and Knoop hardness clearly correlate with each other. The anisotropies of friction, groove width, contact pressure, and Knoop hardness on the {0001}, {10$\bar{1}$0}, and {11$\bar{2}$0} planes of SiC are primarily controlled by the slip system {10$\bar{1}$0} <11$\bar{2}$0> and are explained by a resolved shear stress calculation (refs. 16 to 19).

Figure 6 suggests that the $\langle 10\bar{1}0 \rangle$ directions on the basal plane of SiC which exhibit the lowest coefficient of friction might show the greatest resistance to abrasion resulting from plastic deformation.

To investigate the effect of crystallographic orientation on microfracture, a pyramidal Vickers diamond has been used. Figure 7 shows the variation of total crack length around such an indentation on Mn-Zn ferrite (100), (110), (111), and (211) planes and their Vickers hardness values for experiments at loads of 0.25 to 2.0 N. Measurements were made with one of the diagonals of the Vickers (pyramidal) indentation making angles of approximately 0, 22.5° and 45° to the [011] or (100), [001] on (110), $[11\bar{2}]$ on (111), and $[01\bar{1}]$ on (211). The averages of these three measurements of crack length and hardness are plotted in figure 7. This plot reveals two features of consequence: (1) there exists a crystallographic orientation effect on crack growth and Vickers hardness, and (2) crack growth is linear with increasing load. The cracking of Mn-Zn ferrite was determined to be based on {100} and {110} primary systems. It was also determined that the deformation of Mn-Zn ferrite is controlled by the slip system {110} <110>.

Effects of Tangential Force

In 1891 Auerbach demonstrated that the load for Hertzian cone crack initiation varies linearly with the radius of the indenting sphere (refs. 2 to 7). This relationship, known as Auerbach's law, is of special interest to fracture theorists, (1) because it predicts a size effect, the smaller the indenter, the higher the stress required to initiate fracture, (2) because of its implications concerning the validity of certain brittle fracture criteria, and (3) because of its potential use as a means for measuring fracture surface energies (ref. 5). The theoretical justification of Auerbach's law has consequently been the target of many treatments of Hertzian fracture mechanics.

With a 0.02 mm-radius diamond hemisphere, circular cracks formed on the silicon carbide {0001} surface, when the normal load exceeded 2 N in the indentation process. However, if a tangential force was applied, cracking occurred at the rear of the contact region for a normal load of 0.4 N (ref. 20). Therefore relatively small tangential stresses are very potent in producing conditions for fracture at the surface.

Figure 8 indicates the critical normal load to fracture of Mn-Zn ferrite as a function of radius for both indenter and rider in indentation and in sliding contact. The load to fracture is directly proportional to the radius of the indenter and rider. The tangential force introduced by sliding plays an important role in the generation of surface fracture. With indentation, the cracks produced in the single-crystal Mn-Zn ferrite surfaces were not circular (ring) cracks, but rather extended in radial directions from the indentation. The cracks generated in sliding propagated perpendicular to the sliding direction in the wear tracks.

MICROFRACTURE IN SLIDING CONTACT UNDER ADHESIVE CONDITIONS

The removal of adsorbed films (usually water vapor, carbon monoxide, carbon dioxide, and oxide layers) from the surfaces of ceramics and metals results in very strong interfacial adhesion when two such solids are brought into contact. For example, when an atomically clean silicon carbide surface is brought into contact with a clean metal surface, the adhesive bonds formed at the silicon carbide-to-metal interface are sufficiently strong that fracture of cohesive bonds in the metal and transfer of metal to the silicon carbide surface results (refs. 16 and 20). This is observed in the scanning electron microscope.

Figure 9 presents scanning electron photomicrographs of the wear tracks generated by ten passes of rhodium and titanium riders on the SiC {0001} sur-

face along the <10$\bar{1}$0> direction. Metal transfer is evident in the sliding contact. The sliding of a metal on a silicon carbide surface also results in local cracks along cleavage planes. The cracks, which are observed in the wear tracks, primarily propagate along cleavage planes of the {10$\bar{1}$0} orientation. In figure 9(a), the hexagonal light area is the beginning of a wear track, and there is a large crack where cracks primarily along the {10$\bar{1}$0} planes were generated, propagated and then intersected during loading and sliding of the rhodium rider on the SiC surface. It is postulated from figure 9(a) that subsurface cleavage cracking of the {0001} planes, which are parallel to the sliding surface, also occurs. Figure 9(b) reveals a hexagonal pit and a copious amount of thin titanium film around the pit. The hexagonal fracturing is primarily due to cleavage cracking along {10$\bar{1}$0} planes and subsurface cleavage cracking along the {0001} plane.

Similar fracture pit and multiangular wear debris, having crystallographically oriented sharp edges, have been previously observed with single-crystal Mn-Zn ferrite in contact with itself or a metal (ref. 21). The fracture behavior of the ferrite crystal during sliding was similarly found to be significantly dependent on the cleavage systems of the {110} planes.

Figure 10 presents a scanning electron photomicrograph of the wear track on the silicon carbide {0001} surface generated by single-pass sliding of an iron rider at 800° C in a vacuum of 10^{-8} Pa. The wear track contains microfracture pits in very small areas in the sliding contact region (ref. 8). Under adhesive conditions then, the same two kinds of fracture pits were generally clearly observed as under the abrasive conditions described earlier (figs. 2 and 5), namely: (1) pits with spherically fractured surfaces and (2) pits with polyhedrally fractured surfaces that are nearly of a hexagonal platelet shape. These results reconfirm that spherical fracture may occur

even in single-crystal silicon carbide during sliding. Figure 11 presents a scanning electron photomicrograph of another spherical fracture, showing that a nearly spherically fractured surface can exist in the fracture pit in a very local area of the wear track.

The experimental evidence assembled in this section then allows the conclusion that substantially the same mechanisms operate to produce fracture under adhesive conditions as those described earlier under abrasive conditions.

CONCLUSIONS

From the results of indentation and sliding friction experiments on single-crystal ceramic materials the following conclusions are drawn:

1. Fracture pits with spherically fractured surfaces result from indenting or sliding with hemispherical riders under either abrasive or adhesive conditions. Spherical fracture occurs along the spherical stress trajectories beneath the plastic deformation zone.

2. The same conditions also produce fracture pits with polyhedrally fractured surfaces which are the result of anisotropic fracture. This is primarily controlled by surface and subsurface cracking along cleavage planes.

3. Cracks in Mn-Zn ferrite during indentation elongate linearly with increasing load.

4. Critical normal load to fracture in indentation and sliding is directly proportional to the radius of the hemispherical rider. Tangential forces are very effective in reducing this critical load at the surface of ceramic materials in sliding contact.

5. Primary slip systems of ceramics can explain the anisotropy of friction and plastic deformation observed under abrasive conditions.

REFERENCES

1. Hertz, H., "Ueber die heruhrung fester elastischer karper," Journal für die Reine und Angewandte Mathematik (Berlin), vol. 92, 1881, pp. 156-171.
2. Auerbach, F., Anna. Phys. Chemie., vol. 43, 1891, p. 61. (Also Annales der Physik (Leipzig).)
3. Johnson, O. W., "Damage Produced in Ge at Room Temperature by Indentation," J. Appl. Phys., vol. 37, no. 7, June 1966, pp. 2521-2526.
4. Powell, B. D., and Tabor, D., "The Fracture of Titanium Carbide Under Static and Sliding Contact," J. Phys., vol. 3, 1970, pp. 783-788.
5. Frank, F. C., and Lawn, B. R., "On the Theory of Hertzian Fracture," Proc. R. Soc. (London), vol. A299, 1967, pp. 291-306.
6. Lawn, B. R., "Hertzian Fracture in Single Crystals with the Diamond Structure," J. Appl. Phys., vol. 39, no. 10, Sept. 1968, pp. 4828-4836.
7. Lawn, B. R., and Swain, M. V., "Microfracture Beneath Point Indentations in Brittle Solids," J. Mater. Sci., vol. 10, 1975, pp. 113-122.
8. Miyoshi, K., and Buckley, D. H., "Occurrence of Spherical Ceramic Debris in Indentation and Sliding Contact," NASA TP-2048, 1982.
9. Miyoshi, K., and Buckley, D. H., "The Generation and Morphology of Single-Crystal Silicon Carbide Wear Particles Under Adhesive Conditions," Wear, vol. 67, 1981, pp. 303-319.
10. Preston, F. W., "The Structure of Abraded Glass Surfaces," Trans. Opt. Soc. (London), vol. 23, no. 3, 1922, pp. 141-164.
11. Billinghurst, P. R., Brookes, C. A., and Tabor, D., "The Sliding Process as a Fracture-Inducing Mechanism," Physical Basis of Yield and Fracture, Inst. Phys. Soc. Conf., Ser. 1, 1967, pp. 253-258.

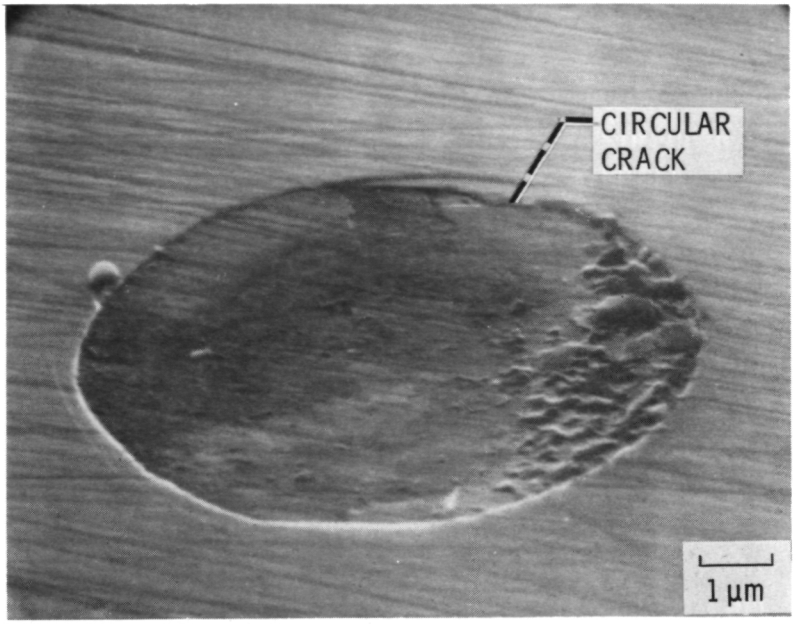

(a) Indentation generated by 0.1-mm-radius hemispherical indenter. Load, 10 N.

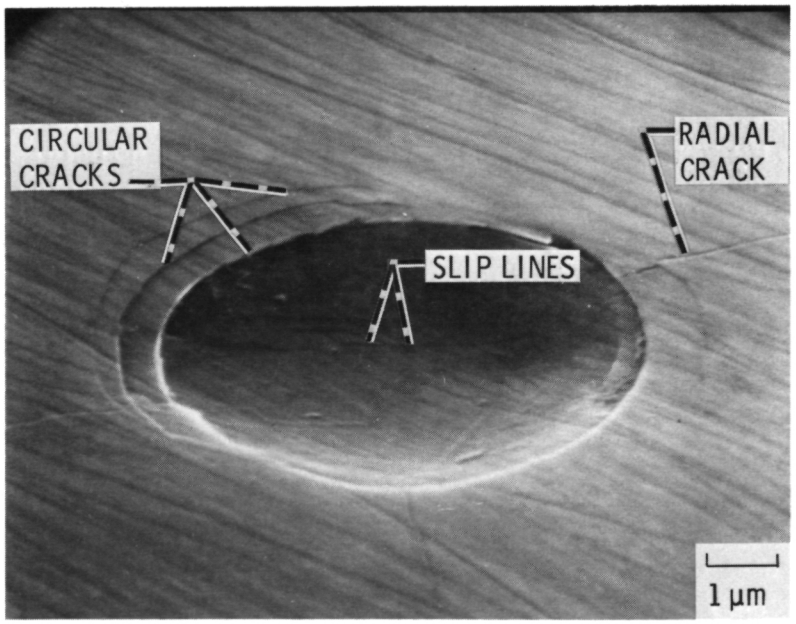

(b) Indentation generated by 0.02-mm-radius hemispherical indenter. Load, 5 N.

Figure 1. - Scanning electron photomicrographs of indentation and cracks on silicon carbide {0001} surface generated by hemispherical indenter.

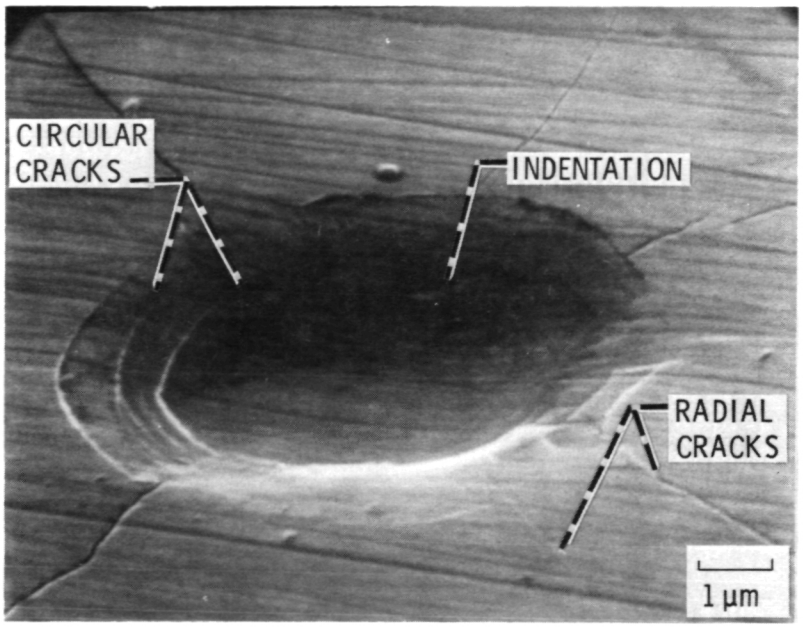

(c) Indentation generated by 0.008-mm-radius hemispherical indenter. Load, 2 N.

Figure 1. - Concluded.

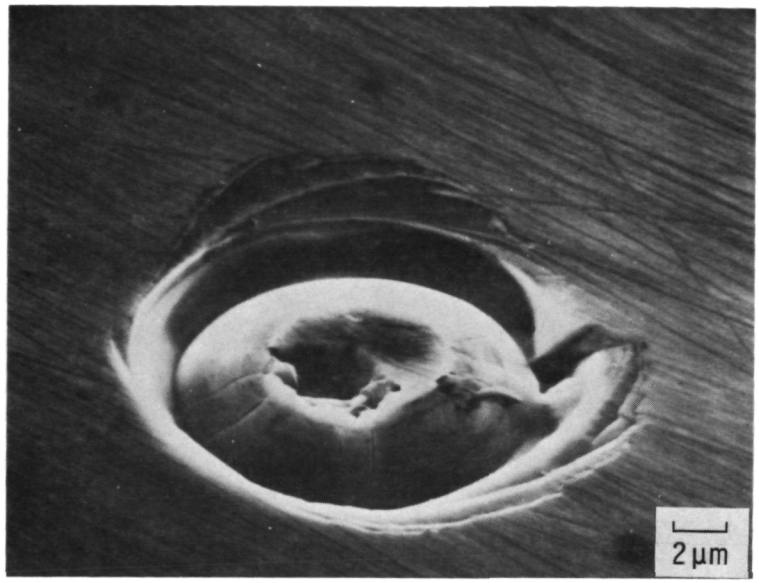

(a) Scanning electron photomicrograph.

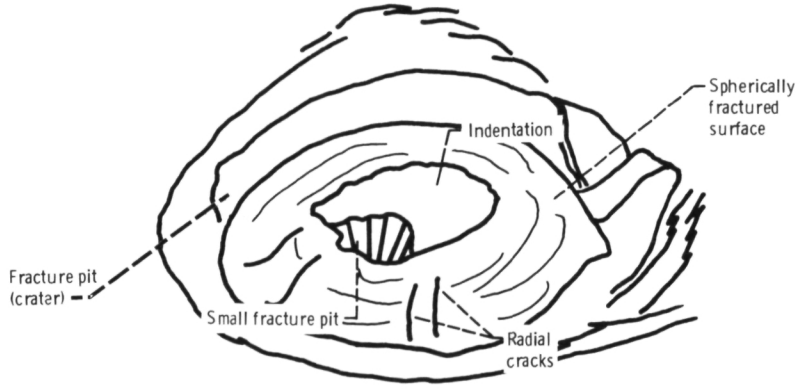

(b) Schematic.

Figure 2. - Indentation and fracture pit with a hemispherically fractured surface generated by 0.008-mm-radius hemispherical indenter. Load, 10 N.

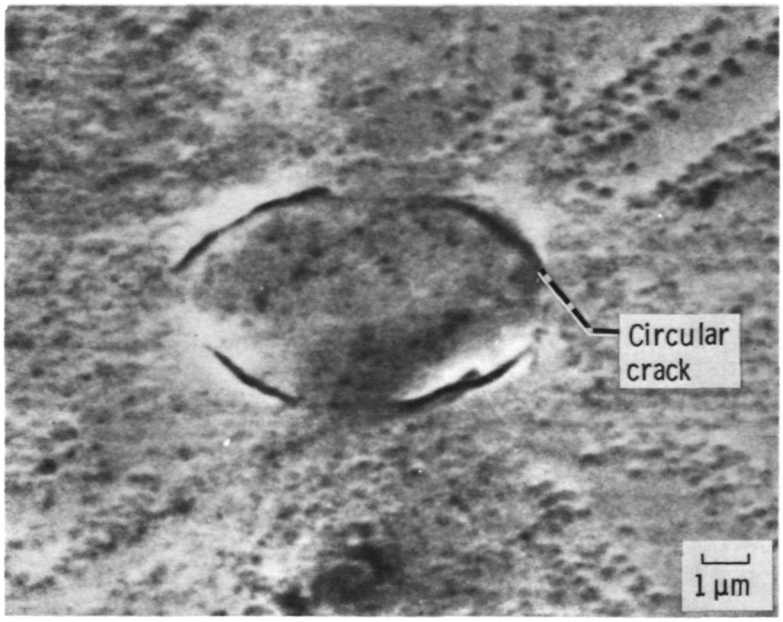

(a) In air.

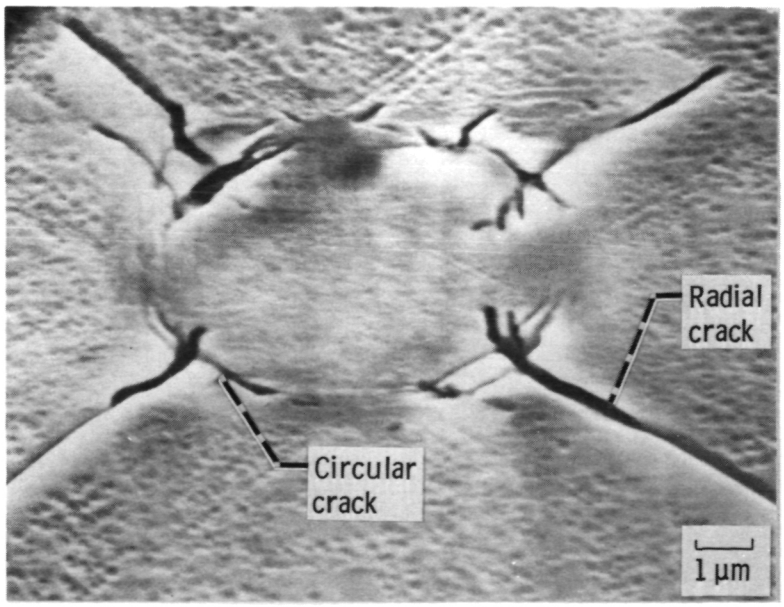

(b) In mineral oil with sulfur additive.

Figure 3. - Scanning electron photomicrographs of indentation and cracks on single-crystal magnesium oxide {001} surface generated by 0.02-mm-radius hemispherical diamond indenter. MgO crystals cleaved in air and in mineral oil with sulfur additive. Indentations made on surface in air or immersed in the oil. Load, 0.25 N; room temperature.

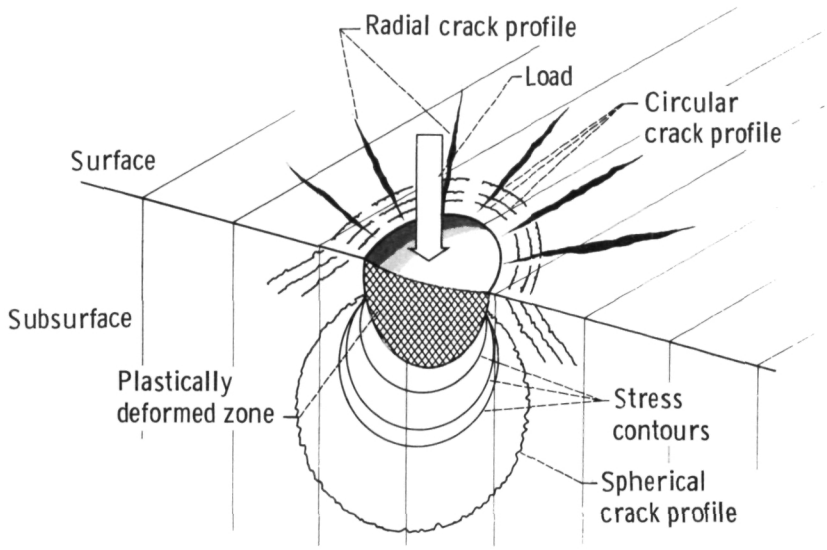

Figure 4. - Schematic of a hemispherical crack formation under plastically deformed zone.

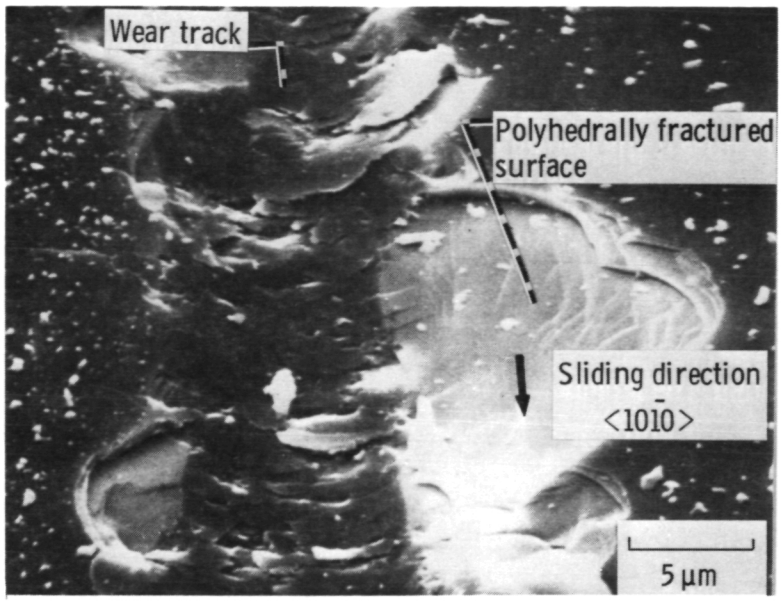

(a) Silicon carbide. Load, 2 N.

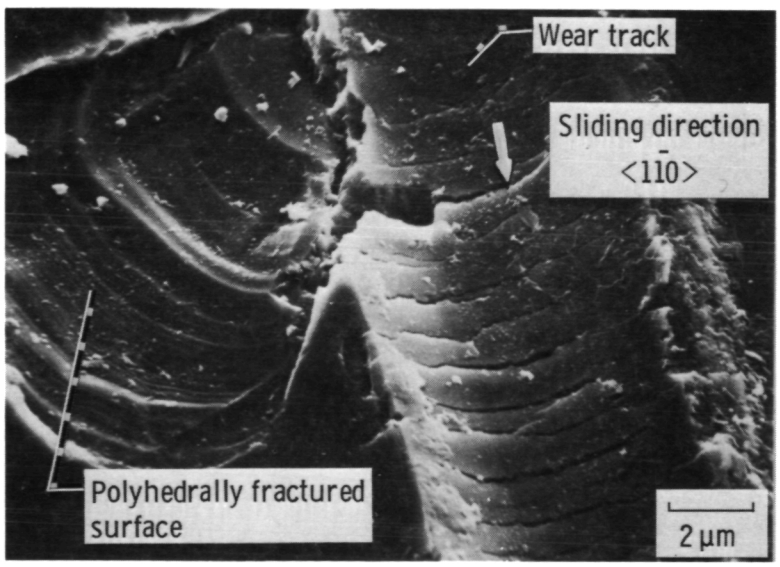

(b) Mn-Zn ferrite. Load, 1 N.

Figure 5. - Scanning electron photomicrographs of wear tracks on single-crystal silicon carbide {0001} surface and manganese-zinc ferrite {110} surface generated by 0.02-mm-radius hemispherical riders.

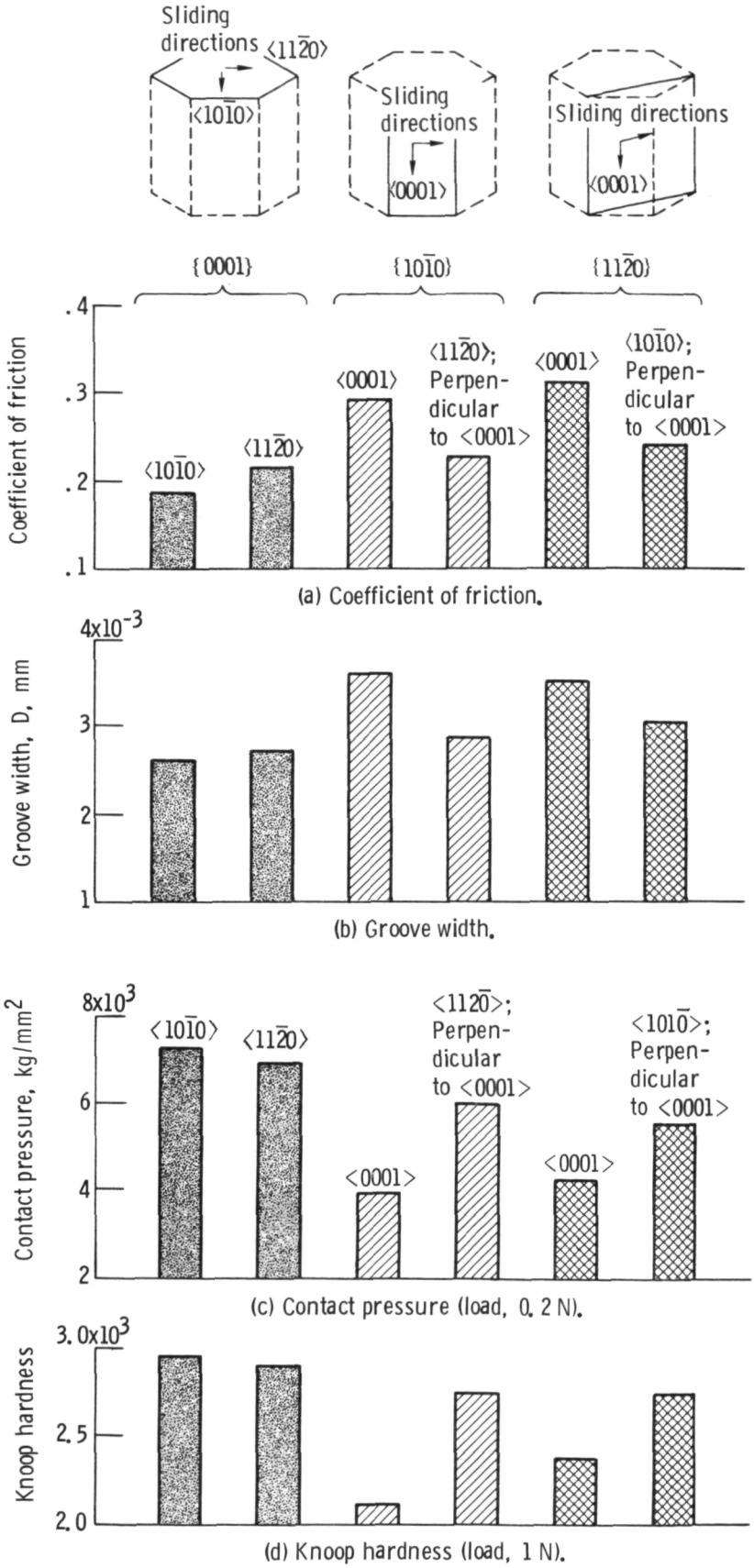

Figure 6. - Anisotropies on {0001}, {10$\bar{1}$0}, and {11$\bar{2}$0} surfaces of SiC.

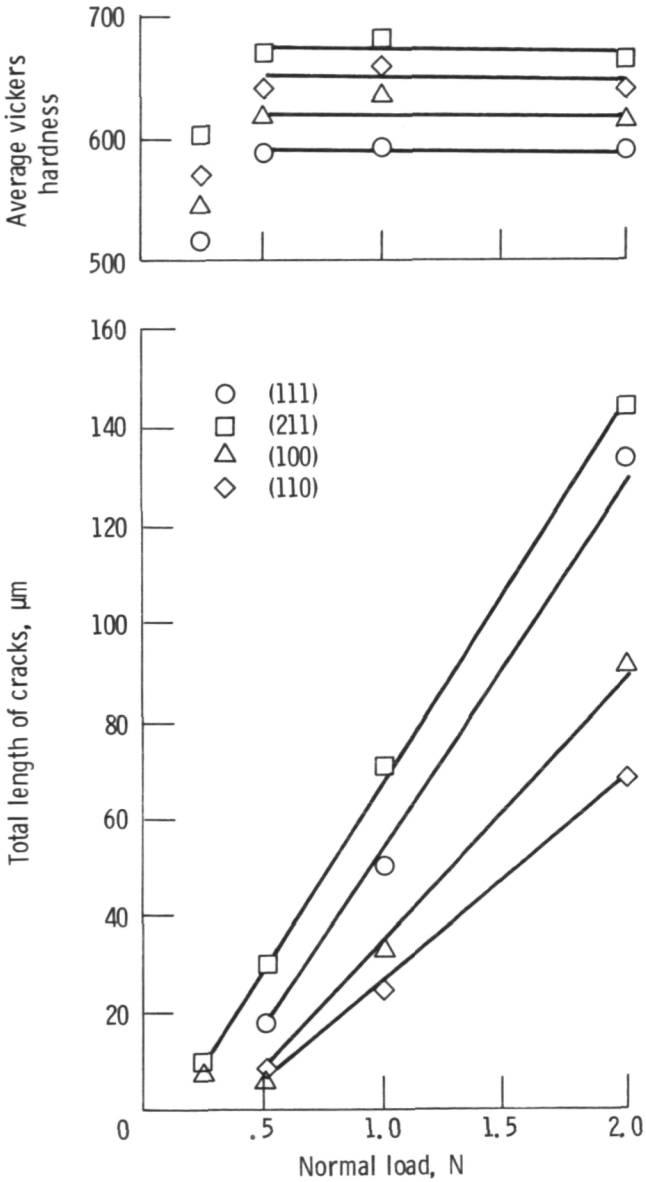

Figure 7. - Anisotropies of crack length and hardness for Vickers indentation on (100), (110), (111) and (211) surfaces of Mn-Zn ferrite.

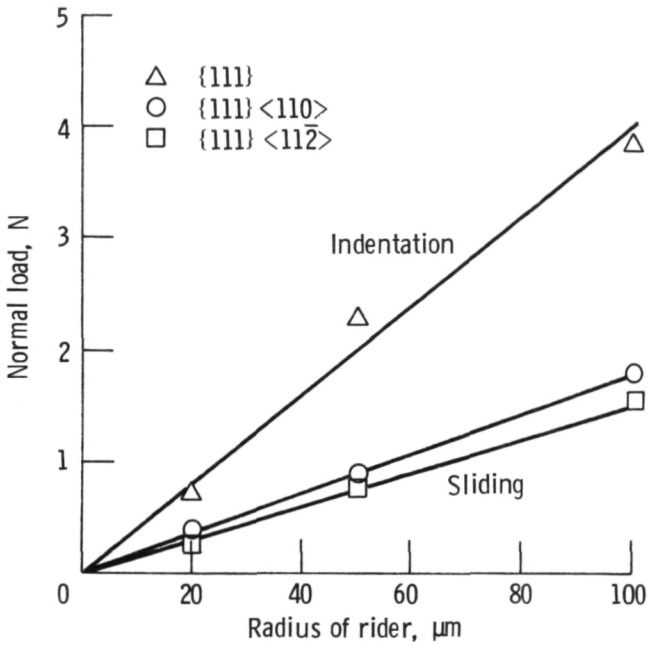

Figure 8. - Critical normal load to fracture of Mn-Zn ferrite as a function of radius of indenter and rider in indentation and in sliding contact. Indentation: {111} surfaces. Sliding: {111} surface, <110> direction; {111} surface, <11$\bar{2}$> direction.

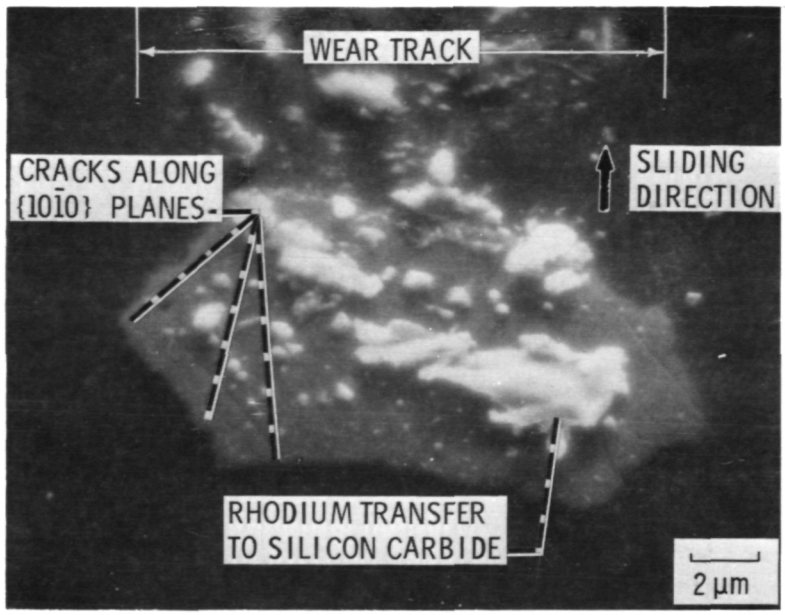

(a) Hexagonal cracking.

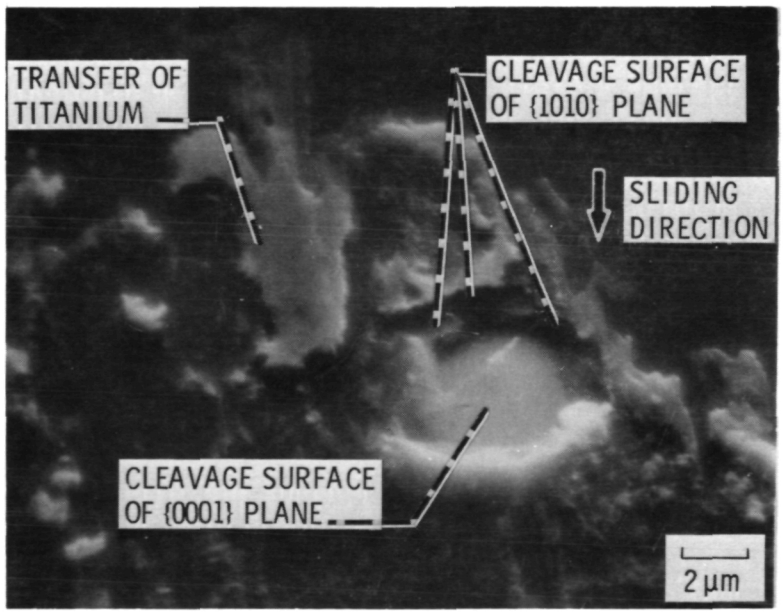

(b) Hexagonal pit.

Figure 9. - Scanning electron photomicrographs of wear tracks on the {0001} surface of single-crystal SiC in contact with rhodium and titanium as a result of ten passes of a rider in vacuum. Sliding direction, <10$\bar{1}$0>; sliding velocity, 3 mm/min^{-1}; load, 0.3 N; room temperature; pressure, 10^{-8} Pa; metal pin rider, 0.79 mm radius.

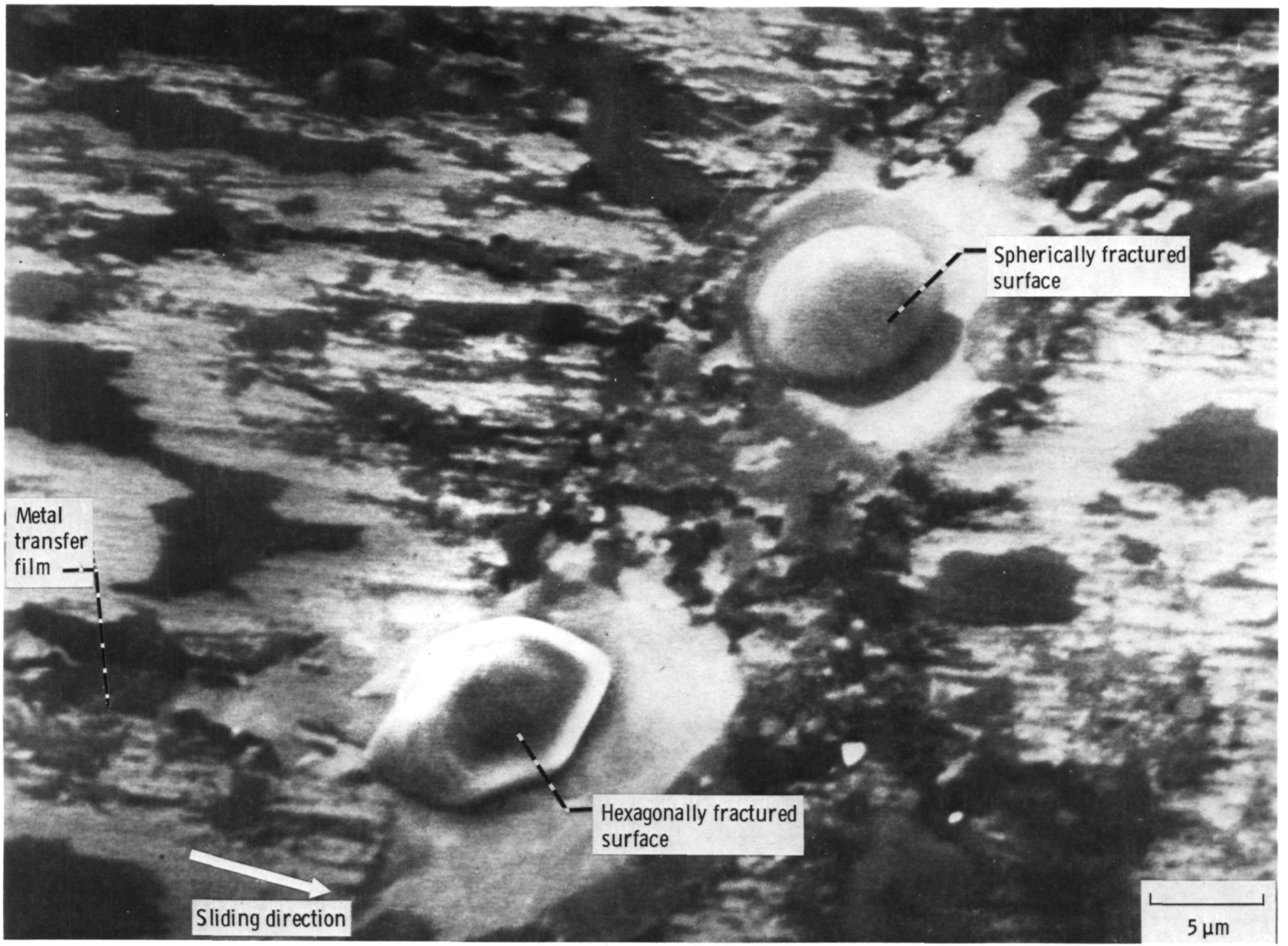

Figure 10. - Wear track with fracture pits on silicon carbide {0001} surface as a result of single-pass sliding of iron rider (0.79 mm radius). Sliding velocity, 3 mm/min; load, 0.2 N; temperature, 800° C; vacuum, 30 nPa.

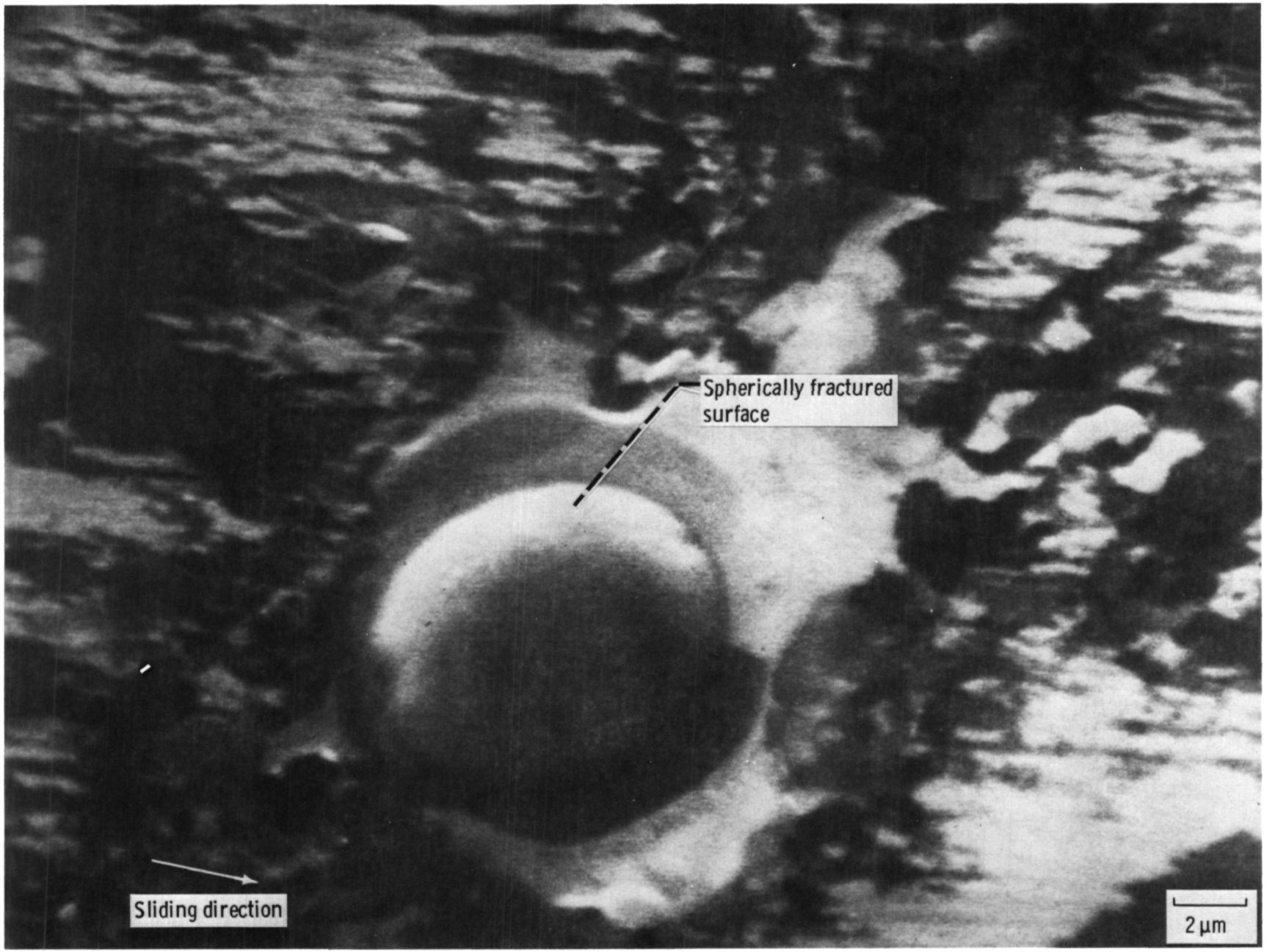

Figure 11. - Fracture pit on silicon carbide {0001} surface with spherically fractured surface as a result of single-pass sliding of iron rider (0.79 mm radius). Sliding velocity, 3 mm/min; load, 0.2 N; temperautre, 800° C; vacuum, 30 nPa.

1. Report No.	2. Government Accession No.	3. Recipient's Catalog No.
NASA TM-83585		

4. Title and Subtitle	5. Report Date
Ceramic Wear in Indentation and Sliding	6. Performing Organization Code 506-53-1B

7. Author(s)	8. Performing Organization Report No.
Kazuhisa Miyoshi and Donald H. Buckley	E-1884
	10. Work Unit No.

9. Performing Organization Name and Address	11. Contract or Grant No.
National Aeronautics and Space Administration Lewis Research Center Cleveland, Ohio 44135	13. Type of Report and Period Covered Technical Memorandum
12. Sponsoring Agency Name and Address	14. Sponsoring Agency Code
National Aeronautics and Space Administration Washington, D.C. 20546	

15. Supplementary Notes

Prepared for the Thirty-ninth Annual Meeting of the American Society of Lubrication Engineers, Chicago, Illinois, May 7-10, 1984.

16. Abstract

This paper discusses the various wear mechanisms involved with single-crystal ceramic materials in indentation and in sliding contacts. Experiments simulating interfacial events have been conducted with hemispherical, conical and pyramidal indenters (riders). With spherical riders, under either abrasive or adhesive conditions, two types of fracture pits have been observed. First, spherical-shaped fracture pits and wear particles are found as a result of either indenting or sliding. These are shown to be due to a spherical-shaped fracture along the circular or spherical stress trajectories. Second, polyhedral fracture pits and debris, produced by anisotropic fracture, are also found both during indenting and sliding. These are primarily controlled by surface and subsurface cracking along cleavage planes. Several quantitative results have also been obtained from this work. For example, using a pyramidal diamond, crack length of Mn-Zn ferrite in the indentation process grows linearly with increasing normal load. Moreover, the critical load to fracture both in indentation and sliding is essentially isotropic and is found to be directly proportional to the indenter radius. Finally, the tangential forces present during sliding are very potent in producing conditions for fracture at the surface. Under such conditions, the observed anisotropy of friction and plastic deformation is explained on the basis of the primary slip systems of these ceramics.

17. Key Words (Suggested by Author(s))	18. Distribution Statement
Ceramics Wear Indentation	Unclassified - unlimited STAR Category 27

19. Security Classif. (of this report)	20. Security Classif. (of this page)	21. No. of pages	22. Price*
Unclassified	Unclassified		

*For sale by the National Technical Information Service, Springfield, Virginia 22161

National Aeronautics and
Space Administration

Washington, D.C.
20546

Official Business
Penalty for Private Use, $300

SPECIAL FOURTH CLASS MAIL
BOOK

Postage and Fees Paid
National Aeronautics and
Space Administration
NASA-451

NASA

POSTMASTER

If Undeliverable (Section 158
Postal Manual) Do Not Return